Title: Humanized archaeal ferritin as a tool for cell targeted delivery

Authors: Valeria de Turris, Matilde Cardoso Trabuco, Giovanna Peruzzi, Alberto Boffi, Claudia Testi, Beatrice Vallone, Linda Celeste Montemiglio, Amedee de Georges, Lorenzo Calisti, Irene Benni, Alessandra Bonamore and Paola Baiocco.

Year: 2017
DOI: 10.1039/c6nr07129e

Nanoscale

Humanized Archaeal ferritin as a tool for cell targeted delivery.

Journal:	*Nanoscale*
Manuscript ID	Draft
Article Type:	Paper
Date Submitted by the Author:	n/a
Complete List of Authors:	De Turris, Valeria; Istituto Italiano di Tecnologia, Center for Life Nano Sciences@Sapienza Cardoso Trabuco, Matilde; Molirom srl Peruzzi, Giovanna; Istituto Italiano di Tecnologia, Center for Life Nano Science@Sapienza Boffi, Alberto; Istituto Italiano di Tecnologia Center for Life Nano Science; Istituto di Biologia e Patologia Molecolari Consiglio Nazionale delle Ricerche Testi, Claudia; Istituto Italiano di Tecnologia, Center for Life Nano Science@Sapienza Vallone, Beatrice; Istituto di Biologia e Patologia Molecolari Consiglio Nazionale delle Ricerche Montemiglio, Linda Celeste; University of Rome Sapienza, Biochemical Sciences de Georges, Amédée; CUNY Advanced Science Research Center Calisti, Lorenzo; University of Rome Sapienza, Biochemical Sciences Benni, Irene; University of Rome Sapienza, Biochemical Sciences Bonamore, Alessandra; University of Rome Sapienza, Biochemical Sciences; Sapienza università di Roma, Baiocco, Paola; Istituto Italiano di Tecnologia Center for Life Nano Science, Center for Life Nano Science

Humanized Archaeal ferritin as a tool for cell targeted delivery.

Valeria de Turris[a], Matilde Cardoso Trabuco[d], Giovanna Peruzzi[a], Alberto Boffi[a,c], Claudia Testi[a], Beatrice Vallone[c], Linda Celeste Montemiglio[b], Amédéede Georges[e], Lorenzo Calisti[b], Irene Benni[b], Alessandra Bonamore[b] and Paola Baiocco[a].

[a.] Center for Life Nano Science@Sapienza, Istituto Italiano di Tecnologia, V.le Regina Elena 291, Rome 00161, Italy

[b.] Department of Biochemical Sciences "Alessandro Rossi Fanelli", Sapienza University of Rome, Rome Italy.

[c.] Institute of Molecular Biology and Pathology, National Research Council, Rome, Italy.

[d.]Molirom srl, via Ravenna 8, 00161, Rome, Italy.

[e.]The City University of New York Advanced Science Research Center 85 St. Nicholas Terrace, New York, NY 10031.

Keywords: Protein cage; Ferritin; cellular uptake; protein crystallography; cryo electron microscopy.

Abstract

Human ferritins have been extensively studied to be used as nanocarriers for diverse applications and could represent a convenient alternative for targeted delivery of anticancer drugs and imaging agents. However the most relevant limitation to their applications is the strong experimental conditions during the particle/cargo assembly. To overcome this issue the unique assembly of *Archaeoglobus fulgidus* ferritin was genetically engineered by changing a surface exposed loop of 12 aminoacids connecting B and C helices to mimic the sequence of the analogous human H-chain ferritin loop. This new chimeric protein was shown to maintain the unique, cations linked, association-dissociation properties of *Archaeoglobus fulgidus* ferritin occurring at neutral pH values, while exhibiting the typical human H-homopolymer recognition by the transferrin receptor TfR1. The chimeric protein was confirmed to be actively and specifically internalized by HeLa cells, thus representing a unique nanotechnological tool for cell-targeted delivery of possible payloads for diagnostic or therapeutic purposes. Moreover, it was demonstrated that the 12 aminoacids loop is necessary and sufficient for binding to the transferrin receptor. The three-dimensional structure of the humanized Archaeoglobus ferritin has been obtained both as crystal by x-ray diffraction and in solution by cryo-EM.

Introduction

Ferritin proteins have been extensively used as nanocarriers for diverse applications due to their hollow cage-like structures and their unique, reversible, 24-mer assembly (1,2). More in detail, they represent the most convenient alternative to viral carriers for targeted delivery of anticancer drugs and imaging agents and have been successfully utilized as reaction nano-vessels for the synthesis of non-native metallic nanoparticles in the inner core, with applications in nanoelectronic devices (3-5). Ferritins external and internal surfaces are chemically and genetically modifiable allowing for the attachment site for drugs, nucleic acids, fluorophores or magnetic moieties. Along this line, recent studies further established heavy (H) or light (L)-chain homopolymers as versatile multifunctional nanocarriers for targeted cancer diagnosis and therapy (6-10). In fact, human ferritins constitute biocompatible nanocarriers that stabilize and shelter the enclosed particles, thus preventing immunogenic responses. Moreover, ferritins are naturally targeted toward ubiquitously expressed TfR1 transferrin receptors (H-chain specific) or hepatic SCARA 5 receptors (L-chain specific). Such properties have been widely exploited for efficient delivery of antitumor drugs to iron avid, fast replicating, tumor cells overexpressing the TfR1 receptor (11). Thus, ferritin based protein cages have been developed as versatile platforms for multiple applications in nanomedicine.

Current development of human ferritin based particle is however facing intrinsic limitations due to the harsh experimental conditions linked to their assembly-disassembly equilibrium, whose control is a prerequisite in order to achieve encapsulation of the cargo within the internal cavity. In the conventional *in vitro* encapsulation procedures, ferritin must be disassembled at extreme pH values and re-assembled in the presence of highly concentrated payload compounds (12). Such a procedure leads to suboptimal load of cargo material, whose chemical structure is required to be pH resistant, and often results in poor payload incorporation yields. Moreover, the pH jump procedure is only partially reversible and re-assembly may not be complete, depending on complex equilibrium and kinetic parameters (13). Extensive research efforts are currently devoted to adjusting the assembly properties of ferritin nanocages to the desired applications either by intersubunit interface mutagenesis (14) or by genetic engineering of N- or C-terminal regions (15).

Recently, novel ferritins from lower eukaryotes, bacteria and archaea, endowed with different polymer association-dissociation thermodynamic and kinetic features have emerged as possible alternatives to human ferritin homopolymers for several biotechnological applications

requiring cargo material encapsulation (16,17). Despite low sequence similarity, these ferritins display a highly conserved quaternary structure consisting of a four-helix bundle namely A, B, C and D and a short E helix at the C-terminus. Helices B and C are connected by a 12 aminoacids (aa) long loop involved in stabilizing interactions at the 2-fold dimer interface. Unlike most eukaryotic and prokaryotic ferritins, the archaeal ferritin from Archaeoglobus *fulgidus* (AfFt) is characterized by unique self-assembly properties. In fact, in neutral buffers it is present as dimeric species, easily combining into a non-canonical 24-mer cage in the presence of metal cations (18). AfFt assembles in a distinctive tetrahedral geometry as a result of particular packing between four hexametric units into a 24-mer structure different from those observed so far. Such unusual assembly results in the formation of four wide triangular pores (45 Å) on the protein shell (19). As demonstrated by Sana *et al*., (19) aminoacid substitutions in the turn motif that connects D and E helices forming the 4-fold iron channels, namely K150A and R151A, are sufficient to restore the canonical octahedral symmetry observed in vertebrate and bacterial ferritins (18,19), thus providing a rationale for the atypical tetrahedral architecture of AfFt. Nevertheless, the low sequence similarity of AfFt with mammalian ferritins runs against the possibility of targeting AfFt onto the TfR1 receptors in mammalian cells.

Transferrin receptor TfR1, or CD71, has been reported to be a preferred target for human ferritin, due to the specific interaction of the receptor extracellular moiety with epitopes of the H-ferritin subunit (20,21). Inspection of the three-dimensional structure of the human H-homopolymer external surface indicates that the most significant accessible area is occupied by the external 12 aa long loop connecting B and C helices (up to 19 aa including the turn regions). Patches of a lesser extent exposed to solvent, are formed by the N-terminal regions or by the iron channels within the threefold axis of the intersubunit assembly. However, it has been shown that that N-terminal or C-terminal deleted human H-homopolymers are efficiently uptaken by target cells, thus suggesting these regions are not relevant for receptor recognition or uptake (22). Therefore the BC loop, besides their structural role in stabilization of interdimer interface (23), appeared to be the best candidate for TfR1 receptor recognition of ferritin molecule.

We decided then to engineer the archaeal ferritin to devise a chimeric construct, named humanized *Archaeoglobus* ferritin (HumAfFt), in which the external 12 aa loop connecting the B and C helices was mutated to reproduce the analogous one in the corresponding region of the human H chain homopolymer (HuHF). It was observed that this chimeric protein (HumAfFt) was actively internalized by HeLa cells to an extent comparable to transferrin, the preferred ligand for TfR1.

RESULTS AND DISCUSSION

"Humanized"Archaeoglobus ferritin design.

Heavy chain human ferritin and *Archaeoglobus* ferritin display 31% sequence identity. The structural alignment of HuHF and AfFt monomers (pdb code 3AJO and 1S3Q, respectively) reveals a shorter N-terminus and shorter loops between three of the four helices, with the notable exception of the long loop connecting B and C helices.

As shown in Fig. 1, the BC loops of two adjacent subunits run in an antiparallel fashion establishing significant, mutual interactions. Thus BC loops of adjacent subunits display the same overall geometry in both HuHF and AfFt, though each couple of loops adopts a different symmetry along the spherical surface of the protein cage, given the different dimer-dimer positioning within each complete 24-mer structure.

In order to preserve the unique assembly properties of AfFt, while implementing a potential cellular uptake, we decided to exploit this external loop by mutating 9 residues into the corresponding residues found in HuHF, according to the sequence alignment shown in Fig. 2. In particular, the nine aminoacids sequence IFLQDIKKP, typical of human H ferritin homopolymer, and located at the center of the 12 aa loop was inserted in place of the VKLYAVEEP (from residue 70 to 79 in AfFt numbering, see Fig. 2). In addition, a cysteine residue in position 54 (AfFt numbering) has been introduced by point mutation in order to provide a conjugation site of potential thiol reactive derivatives into the cavity. As previously noted, we will refer to the chimeric protein described above as humanized Archaeoglobus ferritin (HumAfFt).

Self-assembly assessment.

The effect of mutations on the $MgCl_2$-mediated self-assembly of HumAfFt was studied by size exclusion chromatography (SEC), in order to separate different possible oligomers according to their molecular size. Identical peak-positions confirmed that HumAfFt retains the $MgCl_2$-mediated self-assembly property of native AfFt (see FigS2). As shown in the chromatograms, the increasing of $MgCl_2$ concentration triggered the dimers self-assembly until they reached a stable polymeric structure around 500 kDa, roughly corresponding to the expected 24-mer cage-like structure, at 20 mM $MgCl_2$. The data highlighted that the chimeric HumAfFt maintained the cation induced association/dissociation properties of archaeal ferritin and is possibly assembled into a 24-mer typical structure.

X-ray diffraction data on HumAfFt show the Archaeal ferritins tetrahedral symmetry.

The humanized AfFt crystallized under different conditions with respect to wild type AfFt crystals were exposed to the synchrotron light in order to confirm the tetrahedral symmetry reported for archaeal ferritins. The protein was crystallized in the presence of Mg^{2+} in order to maintain the 24-mer assembly.

The structure of HumAfFt has been determined by X-ray crystallography at a 2.87 Å resolution. It crystallized in the $C222_1$ space group, as observed also for wild type AfFt. The asymmetric unit (ASU) contains 12 identical subunits with a solvent content of 64,3 %. The overall folding corresponded to the wild type structure (pdb code 1S3Q) with a rmsd value of 0.4 Å and displayed four wide triangular pores on the surface (Fig 1A). B factors analysis shows a mean B factor of 66 $Å^2$ with the exception of the loop region between the D and E helices, which displays higher B factors and a poor electron density on the side chains from 146 to 151 residues. Conversely, the BC loop is well organized and the analysis of the difference electron density (Fo-Fc) map clearly showed the presence of the mutated residues in the loop between helices B and C as well as the M54C mutation, pointing towards the inner cavity.

Two magnesium ions have been positioned and successfully refined in the ASU, and they are located in the ferroxidasic site of two different subunits. In both, one magnesium ion is coordinated with both OE1 and OE2 of Glu19, (at 2.5 Å and 2.8 Å distance, respectively), with Glu52 (OE1) at 2.5 Å, with Gln129 (OE1) at 2.6 Å and with a water molecule at 2.6 Å distance. In the other chains, a water molecule has been modelled in the Fo-Fc map and successfully refined in the same position.

The loop region, including the conserved terminal turns, spans from aminoacid 68 to aminoacid 86. The sequence alignment and the structural superposition between HumAfFt and the human H-homopolymer, as well as between HumAfFt and AfFt, are shown in Fig. 2B and 2C. At the dimeric interface between the two antiparallel BC loops, the main interactions are a hydrogen bond between Arg69(NH2) and Ser80 (O) at 2.8Å distance and two salt bridges, namely Lys71 (NZ) - Glu77 (OE1) at 3.0Å distance and Glu81 (OE2)-Arg69 (NH1) at 2.7Å distance. A weak salt bridge is established by Glu81 (OE2) and Arg69 (NH2), at a distance of 3.0Å. The salt bridge between Lys71 and Glu77 observed in HuHF, is absent in HumAfFt since these positions were mutated into a phenylalanine (Phe71) and a lysine (Lys77). Other interactions are conserved between HuHF and HumAfFt and displayed the same distances.

Cryo-Electron Microscopy confirms the canonical AfFt architecture in solution.

Humanized AfFt samples were prepared in thin ice layer and analyzed by cryo-EM in order to assess the three-dimensional structure of the chimeric protein in a near-native environment. Particles were picked with the reference-based automated particle picking procedure. Single ferritin

particles were visualized at a nominal resolution of 33 Å demonstrating that their shape and dimensions correspond to that of wild type AfFt in its 24-mer assembly (Fig 3A). Moreover, the triangular apertures on the protein surface were clearly observable in a bi-dimensional view (Fig. 3B) and better displayed in a three-dimensional reconstruction shown in Fig 3C.

Flow cytometry analysis shows HumAfFt cellular uptake.

After we have demonstrated that our HumAfFt maintained the structure with large open pores and the self-assembly propriety characteristic of the original AfFt, we aimed to verify that the modified version also gained access to eukaryotic cancer cells such as HeLa cells. It is known that HuHF is recognized and internalized by the TfR1, which is overexpressed in many types of tumor cells but not in normal cells and healthy tissues (21). To validate the effect of our mutations on the external loop related to the uptake efficiency by HeLa cells, we performed time course experiments on cells treated with the same amount (30μg/μL) of AfFt-FITC, HumAfFt-FITC and transferrin-FITC (TF-FITC) and analyzed them by flow cytometry. As a baseline for FITC fluorescence, control cells not incubated with FITC-ferritins were used. Moreover, to exclude any signal generated from outside particles sticking on the cell membrane due to unspecific binding or remains from the washing steps, Trypan blue quenching was performed before FACS acquisition. In Figure 4, the FACS analysis is summarized, shown as the percentage of cells internalizing the nanoparticles at different time. These data highlighted that HumAfFt nanoparticles are efficiently uptaken by HeLa cells already after one hour incubation with a much higher percentage compared to AfFt (81% and 5% respectively). After longer incubation time (20 hours) the cell FITC-positive for the humanized are increased at more than 90% whereas for the native AfFt are still less than 20%. The latter increment is possibly due to unspecific uptake by pinocytosis. Each acquisition plot is shown in FigS4.

Visualization of ferritin nanoparticles inside living cells by confocal microscopy

In order to visualize uptaken HumAfFt-FITC nanocages, we performed the internalization assay directly on the ibidi 8-well μ-slide and incubated the cells for 20 hours before confocal microscopy. We exploited the properties of a HeLa TagRFP cell lines available in the lab in order to have a reference fluorescent signal confirming that we were imaging inside the cell. This cell line contains a TagRFP-FUS protein under the control of a doxycycline-inducible promoter that allows for a controlled expression of the protein and hence permits visualization of the nucleus in the red channel. In this case the cells were not selected to eliminate the untransfected cells, letting us to visualize different level of expression and also unstained nuclei. Just before imaging, cells were

washed to eliminate the unbound FITC-nanoparticles and then acquired by confocal laser-scanning microscopy. Confocal representative images of entire field of view of live HeLa TagRFP cells alone (control) or incubated with HumAfFt-FITC or TF-FITC are shown in Fig. 5A. Detailed views of the boxed region in panel A are shown in Fig. 5B. Images confirmed the high extent of HumAfFt internalization and highlight a cellular distribution in the cytoplasm and in the perinuclear space comparable to that observed in the case of transferrin, thus suggesting a typical clathrin-coated endocytosis pathway, possibly mediated by TfR1.

Conclusion

The present data highlight remarkable properties of a novel chimeric ferritin nanocage suitable for the design of efficient and versatile scaffolds for intracellular delivery of bioactive small molecules and/or diagnostic probes. *Archaeoglobus fulgidus* ferritin (AfFt) is a prominent example of this versatility due to its unique association/dissociation properties that lead to the presence of stable dimeric species at neutral pH and low ionic strength capable of associating into non-classical 24-mer species in the presence of either monovalent or divalent cations at physiological concentrations (*i.e.* higher than 0.5 M Na^{+}or 20 mM Mg^{++}). Moreover, AfFt also displays a unique subunit assembly, based on tetrahedral symmetry, which leads to the formation of four large openings in the protein shell. As such, AfFt represents a uniquely suitable scaffold for incorporating a wealth of diverse substructures inside the protein cavity, either by assembly/disassembly process at neutral pH or by diffusion through the large triangular pores on the surface. Notable examples have been reported in recent literature (17). Nevertheless, one of the key properties of ferritin nanocages in biomedical applications is the possibility of targeting receptors on human cells, thus allowing the delivery of the desired payload within the cytoplasm. The engineered HumAfFt here described combines the versatility in assembly and cargo incorporation of AfFt with binding to TfR1 and cellular uptake of HuHF.

Materials and Methods:

"Humanized" Archaeoglobus ferritin design.

The gene encoding for a mutated ferritin from *Archaeoglobus fulgidus* was synthesised by GeneArt (ThermoFisher) and subcloned into a pET22b vector (Novagen) between the restriction sites NdeI and HindIII at 5' and 3' respectively. The recombinant plasmid was transformed into BL21(DE3) *E. coli* strain for protein expression.

Protein Expression and Purification.

E. coli cells containing HumAfFt plasmid, were grown and induced with 1 mM IPTG (Isopropyl-β-D-1-thiogalactopyranoside) at OD_{600}=0.6. Cells were harvested by centrifugation 3 hours post induction at 37°C.

Cells harvested from 1 L culture were resuspended in 20 mM HEPES buffer, pH 7.5, containing 200 mMNaCl, 1 mM TCEP (tris(2-carboxiethyl)phosphine), and a cOmpleteTM Mini Protease Inhibitor Cocktail Tablet (Roche). Cells were disrupted by sonication and the soluble fraction was purified by heat treatment at 78°C for 10 minutes. Denatured *E. coli* proteins were removed by centrifugation at 15,000 rpm at 4°C for 1 hour. The soluble protein was further purified by ammonium sulfate precipitation. The precipitated fraction at 70% ammonium sulfate, was resuspended in 20 mM HEPES, 50 mM $MgCl_2$, pH 7.5 and dialyzed versus the same buffer. As final purification step, the protein was loaded onto a HiLoad 26/600 Superdex 200 pg column previously equilibrated in the same buffer using an ÄKTA-Prime system (GE Healthcare). Purified protein was concentrated to obtain the final protein preparation of 1 mg/mL and protein concentration was calculated by measuring the UV spectrum using an extinction coefficient of 32400 $M^{-1}cm^{-1}$. Protein yield was ~40 mg/L culture.

Self-assembly assessment in solution.

Size exclusion chromatography $MgCl_2$-mediated self-assembly was studied by size exclusion chromatography (SEC) using Superdex 200 26/600 GL column (GE Healthcare). Molecular size of HumAfFt was determined at different conditions by comparing the elution volume with that of standard proteins. Composition of the mobile phase was 25 mM HEPES pH=7.5 with different $MgCl_2$ concentrations accordingly to the composition of the protein buffer.

Crystallization and crystal structure determination.

Purified protein has been concentrated at 20 mg/mL and initial crystallization screening was performed using a Phenix Robot. Crystals were obtained by mixing in a 2µL hanging drop 1mM of purified protein with a solution containing 22% (vol/vol) polyacrylic acid PAA, 0.1 M Tris, 0.02 M $MgCl_2$, pH 7.4, at 25°C within a week, cryo-protected by increasing the precipitant concentration and flash-frozen in liquid nitrogen. Diffraction data have been collected at ID23-2 beamline at the European Synchrotron Radiation Facility (ESRF), Grenoble, France.

Data were processed with XDS (24) and scaled with Aimless (ccp4 suite) at a final resolution of 2.87 Å. The structure was solved by Molecular Replacement with MolRep (ccp4 suite) using the open pore structure AfFt (pdb code 1S3Q) as search model. Model Building and refinement were done using Coot (25) and Refmac5, respectively. The final model was analyzed with PROCHECK (26) and Molprobity (27). Ramachandran Plot showed that 97.8 % residues are

in preferred regions, 2,2 % in allowed regions and no outlier is observed. The final atomic coordinates and structure factors were deposited with the PDB Data Bank (www.rcsb.org) with accession code (5LS9). Complete data collection and refinement statistics are reported in Table S1.

CryoElectron microscopy.

Holey-gold grids were prepared as described by Russo and Passmore (28) from Quantifoil R1.2/1.3 (Quantifoil Micro Tools GmbH, Germany). 3µL of HumAfFt (12 µM) was applied to the holey-gold grids after plasma cleaning with a mixture of H_2 and O_2. Grids were blotted for 4 seconds and vitrified by rapidly plunging into liquid ethane at −180°C (29, 30) with a Vitrobot (FEI).

Data acquisition was done on a FEI Titan Halo (FEI, Eindhoven) operating at 300 kV. Datasets were imaged with a Volta phase-plate (FEI, Eindhoven) (Danev et al., 2014) and were collected with the automated data collection system EPU (FEI, Eindhoven) at a nominal magnification of 59,000× on an FEI Ceta camera (FEI, Eindhoven) with a camera pixel size of 14 µm, corresponding to a calibrated pixel size of 1.49 Å on the specimen scale and with a dose of 50 $e^-/Å^2$.

Image processing. The particles were picked with the reference-based automated particle picking procedure implemented in RELION 1.3 (31, 32). CTF correction was not applied since the data were collected within 200 nm of focus and the first CTF zero crossing was well beyond the achievable resolution of the dataset. Those particles were subjected to 2D classification using RELION with k=100 classes. Good particles were then subjected to 3D classification using RELION with the number of classes *K*=8. Resulting classes were refined with the autorefine procedure in RELION.

Resolution estimation. Reported resolutions are based on the 'gold-standard' protocol with the FSC=0.143 criterion using soft masks with a 8 pixel soft edge, and were corrected for the effects of the mask on the FSC curve using high-resolution noise substitution (32).

Maps were visualized using UCSF Chimera (33).

Cell lines generation

The HeLa cell line stably expressing an inducible TagRFP-FUS protein (HeLaTagRFP) was generated by transfection with epB-Puro-TT-RFP-FUS wt plasmid and the epiggyBac transposase vector. Plasmid construction is described in ref. (34).

Protein FITC labeling

HumAfFt, AfFt and Olo-transferrin were labeled with Fluorescein-isothiocyanide (ThermoFisher) according to the manufacturer's standard protocol. Briefly, 2 mg/mL of purified protein was added with 10-fold molar excess of in protein storage buffer stirring for 2 hours at RT. The non-reacted dye was removed by gel filtration chromatography and fluorescent dye to protein ratio was determined by UV-spectroscopy. All proteins resulted >95% FITC labeled.

Cell cultures and ferritins internalization

HeLa cells were grow at 37ºC in Eagle's MEM supplemented with 10% (v/v) FBS, Glutamax (Invitrogen) and Penicillin-Streptomycin solution (Sigma). When needed, cells were induced with doxycycline 0.2µg/mL. The internalization assay was performed as follow: after seeding cells on the relevant substrate depending on the experiment, cells were left one day to attach and then incubated with FITC-ferritin nanoparticles (AfFt-FITC, HumAfFt-FITC or Tf-FITC as specified in each experiment) at the final concentration of 30 µg/µL for the time indicated (1h, 3h or 20h).

Flow cytometry analysis

For flow cytometry analysis HeLa cells were seeded on multiwell plates. Cells were incubated with FITC-ferritin nanoparticles as described previously then washed two times with PBS, detached with Trypsin-EDTA (Euroclone), washed with PBS and resuspended in BD-FACS Flow buffer. Half of each sample was treated with Trypan Blue (TB; Sigma) to quench FITC signal from membrane-bound nanoparticles that were not internalized. The quenching was performed with 0.04% TB for 10 min on ice. Control cells were treated in the same way but without FITC-ferritins incubation. Internalization of ferritins before and after TB treatments was measured at the BD LSFORTESSA (BD Biosciences, San Jose, CA, USA) equipped with a 488nm laser and FACSDiva software (BD Biosciences version 6.1.3). Live cells were first gated by forward and side scatter area (FSC-A and SSC-A) plot, then detected in the green channel for FITC expression (530/30nm filter) and side scatter parameter. The gate for the final detection was set in the control sample. Data were analyzed using FlowJo9.3.4 software (Tree Star, Ashland, OR, USA).

Confocal microscopy of live cells

To visualize live cells ferritin internalization by confocal microscope, HeLa TagRFP cells were seeded on the µ-slide 8well ibiTreat (ibidi) and induced with doxycycline 0.2µg/mL. Cells were then incubated with FITC-ferritin nanoparticles as previously described for 20h and, before microscopy acquisition, cells were washed two times with imaging medium (DMEM without

Phenol Red, 10% FBS, 10mM Hepes, Glutamax and Penicillin-Streptomycin solution) to eliminate the unbound FITC-nanoparticles. The confocal laser-scanning microscope was an Olympus FV10i platform equipped with a built-in incubator. Images were acquired with a 60×/1.2NA water-immersion objective, LD lasers 473nm and 559nm and filter sets for FITC and TRITC. Phase-contrast images were acquired simultaneously.

Acknowledgments

We thank Alessandro Rosa and Riccardo De Santis for the HeLa TagRFP cell line. EU H_{2020} Project "X-Probe", Grant N° 637295, to A.B. and M.C.T. is gratefully acknowledged. Flagship Project "Nanomax" to A.B. is also acknowledged.

References

1. Theil EC. Ferritin protein nanocages use ion channels, catalytic sites, and nucleation channels to manage iron/oxygen chemistry. *Curr Opin Chem Biol,* 2011, **15**, 304-311.
2. Schoonen L,van Hest JC., Functionalization of protein-based nanocages for drug delivery applications. *Nanoscale,* 2014, **6**, 7124-41.
3. Prastaro A, Ceci P, Chiancone E, Boffi A, Fabrizi G, and Cacchi S. Homocoupling of arylboronic acids and potassium aryltrifluoroborates catalyzed by protein-stabilized palladium nanoparticles under air in water. *Tetrahedron letters* 2010, **51**, 2550.
4. Meng F, Sana B, Li Y, Liu Y, Lim S, Chen X. Bioengineered tunable memristor based on protein nanocage. *Small* 2014, **10**, 277-83.
5. Kostiainen MA, Hiekkataipale P, Laiho A, Lemieux V, Seitsonen J, Ruokolainen J, Ceci P. Electrostatic assembly of binary nanoparticle superlattices usingprotein cages. *Nat Nanotechnol*., 2013,**8**, 52-56.
6. Liang M, Fan K, Zhou M, Duan D, Zheng J, Yang D, Feng J, Yan XH-ferritin-nanocaged doxorubicin nanoparticles specifically target and kill tumors with a single-dose injection. *Proc Natl Acad Sci* U S A., 2014,**111**,14900-14905.
7. Vannucci L, Falvo E, Failla CM, Carbo M, Fornara M, Canese R, Cecchetti S, Rajsiglova L, Stakheev D, Krizan J, Boffi A, Carpinelli G, Morea V, Ceci P.In Vivo Targeting of Cutaneous Melanoma Using an Melanoma Stimulating Hormone-Engineered Human Protein Cage with Fluorophore and Magnetic Resonance Imaging Tracers. *J Biomed Nanotechnol,*2015,**11**, 81-92.
8. Falvo E, Tremante E, Fraioli R, Leonetti C, Zamparelli C, Boffi A, Morea V, Ceci P, Giacomini P. Antibody-drug conjugates: targeting melanoma with cisplatin encapsulated in protein-cage nanoparticles based on human ferritin. *Nanoscale,* 2013,**5**,12278-12285.
9. Vannucci L, Falvo E, Fornara M, Di Micco P, Benada O, Krizan J, Svoboda J, Hulikova-Capkova K, Morea V, Boffi A, Ceci P. Selective targeting of melanoma by PEG-masked protein-based multifunctional nanoparticles. *Int J Nanomedicine,* 2012, **7**,1489-1509.
10. Geninatti Crich S, Cadenazzi M, Lanzardo S, Conti L, Ruiu R, Alberti D, Cavallo F, Cutrin JC, Aime S. Targeting ferritin receptors for the selectivedelivery of imaging and therapeutic agents to breast cancer cells. *Nanoscale*, 2015,**7**,6527-6533.
11. Fan K, Cao C, Pan Y, Lu D, Yang D, Feng J, Song L, Liang M, Yan X. Magnetoferritin nanoparticles for targeting and visualizing tumour tissues. *Nat Nanotechnol,* 2012,**7**, 459-464.

12. Zhen Z, Tang W, Todd T, Xie J. Ferritins as nanoplatforms for imaging and drug delivery. *Expert Opin Drug Deliv*., 2014, **11**, 1913-22.
13. Kim M, Rho Y, Jin KS, Ahn B, Jung S, Kim H, Ree M. pH-dependent structures of ferritin and apoferritin in solution: disassembly and reassembly. *Biomacromolecules*, 2011,**12**, 1629-40.
14. Chen H, Zhang S, Xu C, Zhao G. Engineering protein interfaces yields ferritin disassembly and reassembly under benign experimental conditions. *Chem Commun (Camb)* 2016, **52**,7402-5.
15. Kim S, Jeon JO, Jun E, Jee J, Jung HK, Lee BH, Kim IS, Kim S. Designing Peptide Bunches on Nanocage for Bispecific or Superaffinity Targeting. *Biomacromolecules*. 2016,**17**,1150-9.
16. Sevcenco AM, Paravidino M, Vrouwenvelder JS, Wolterbeek HT, van Loosdrecht MC, Hagen WR, Phosphate and arsenate removal efficiency by thermostable ferritinenzyme from Pyrococcusfuriosus using radioisotopes. *Water Res*., 2015, **76**, 181-6.
17. Sana B, Johnson E, Lim S. The unique self-assembly/disassembly property of Archaeoglobusfulgidus ferritin and its implications on molecular release from the protein cage. *Biochim Biophys Acta,*2015,**1850**, 2544-2551.
18. Johnson E, Cascio D, Sawaya MR, Gingery M, Schröder I. Crystal structures of a tetrahedral open pore ferritin from the hyperthermophilicarchaeonArchaeoglobusfulgidus. *Structure*, 2005,**13**, 637-648.
19. Sana B, Johnson E, Le Magueres P, Criswell A, Cascio D, Lim S. The role of nonconserved residues of Archaeoglobus fulgidus ferritin on its unique structure and biophysical properties. *J Biol Chem,* 2013,**288**, 32663-32672.
20. Heger Z, Skalickova S, Zitka O, Adam V, Kizek R. Apoferritin applications in nanomedicine. *Nanomedicine* (Lond), 2014, **9**, 2233-45.
21. Li L, Fang CJ, Ryan JC, Niemi EC, Lebrón JA, Björkman PJ, Arase H, Torti FM, Torti SV, Nakamura MC, Seaman WE. Binding and uptake of H-ferritin are mediated by human transferrin receptor-1. *Proc Natl Acad Sci* U S A., 2010,**107**,3505-10.
22. Levi S, Luzzago A, Cesareni G, Cozzi A, Franceschinelli F, Albertini A, Arosio P.Mechanism of ferritin iron uptake: activity of the H-chain and deletion mapping of the ferro-oxidase site. A study of iron uptake and ferroxidase activity of human liver, recombinant H-chain ferritins, and of two H-chain deletion mutants. *J Biol Chem,* 1988,**263**,18086-92.
23. Bernacchioni C, Ghini V, Pozzi C, Di Pisa F, Theil EC, Turano P. Loop electrostatics modulates the intersubunit interactions in ferritin. *ACS Chem Biol*., 2014,**9**, 2517-25.
24. Kabsch W., Integration, scaling, space-group assignment and post-refinement. *Acta Crystallogr D Biol Crystallogr*. 2010,**66**, 133-44.
25. Emsley P, Cowtan K. Coot: model-building tools for molecular graphics. *Acta Crystallogr D Biol Crystallogr.*, 2004,**60**, 2126–2132.
26. Laskowski R A, MacArthur M W, Moss D S, Thornton J M . PROCHECK - a program to check the stereochemical quality of protein structures. *J. App. Cryst.*,1993, **26**, 283-29125.
27. Chen VB, Arendall WB 3rd, Headd JJ, Keedy DA, Immormino RM, Kapral GJ, Murray LW, Richardson JS, Richardson DCMolProbity: all-atom structure validation for macromolecular crystallography. *Acta Crystallographica D,* 2010, **66**, 12-21.
28. Russo CJ, Passmore LA. Ultrastable gold substrates for electron cryomicroscopy. *Science*, 2014,**346**, 1377–1380.
29. Dubochet J, Adrian M, Chang JJ, Homo JC, Lepault J, McDowall AW, Schultz P. Cryo-electron microscopy of vitrified specimens. *Quarterly Reviews of Biophysics,* 1988,**21**, 129–228.
30. Wagenknecht T, Grassucci R, Frank J.Electron microscopy and computer image averaging of

ice-embedded large ribosomal subunits from Escherichia coli. *J. Mol. Biol.*, 1988,**199**, 137–147.
31. Scheres, SHW. Semi-automated selection of cryo-EM particles in RELION-1.3. *J. Struct. Biol*., 2015,**189**, 114–122.
32. Chen S, McMullan G, Faruqi AR, Murshudov GN, Short JM, Scheres SH, Henderson R. High-resolution noise substitution to measure overfitting and validate resolution in 3D structure determination by single particle electron cryomicroscopy.*Ultramicroscopy,* 2013, **135**, 24–35.
33. Pettersen EF, Goddard TD, Huang CC, Couch GS, Greenblatt DM, Meng EC, Ferrin TE. UCSF Chimera--a visualization system for exploratory research and analysis. *J Comput Chem*, 2004, **25**, 1605–1612.
34. Morlando M, Dini Modigliani S, Torrelli G, Rosa A, Di Carlo V, Caffarelli E, Bozzoni I. FUS stimulates microRNA biogenesis by facilitating co-transcriptional Drosha recruitment. *EMBO J*., 2012,**31**, 4502.
35. Robert, X. and Gouet, P. Deciphering key features in protein structures with the new ENDscript server. *Nucleic Acids Res*., 2014,**42**, 320-4

Table of Content:

Coupling Archaea and Human properties into one protein: a new chimeric ferritin.

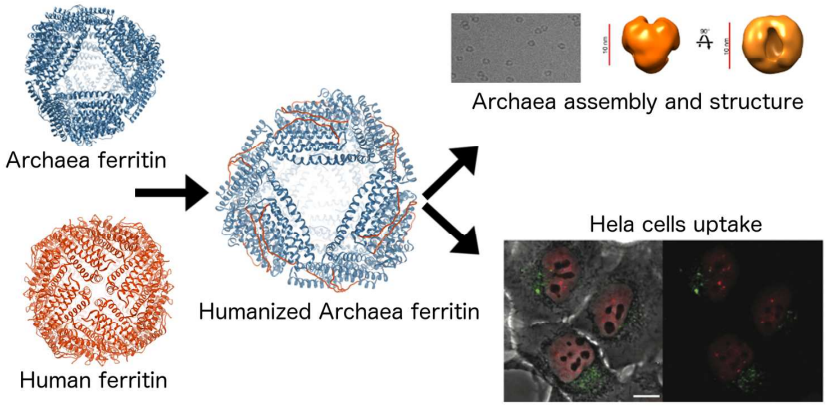

FIGURE LEGENDS

Fig 1: Three-dimensional structures determined by X-ray Crystallography.
A cartoon representation of A) HumAfFt and B) HuHF (pdb code 3AJO). Models are coloured in blue and green, respectively and external loop connecting helices B and C of each monomer is shown in red ribbon. Molecular graphics were performed using UCSF Chimera package (33).

Fig 2: Structure-Based Sequence Alignment of AfFt, HumAfFt, and HuHF.
A) Close-up view of the sequence alignment. Elements of secondary structure for the AfFt are shown on the top. White characters in a red background indicate strict conservation while residues with poor conservation are drawn in black on a white background. Alignments were made using CLUSTAL Omega, and the figure was generated using ENDSCRIPT (35). The structural superposition of the region from R69 and S84 (AfFt numbering) is shown in B) HumAfFt (in blue) *vs.* HuHF (in yellow) and in C) HumAfFt (in blue) *vs.*AfFt (in orange). Residues are depicted as sticks coloured by atom, N in blue, O in red and S in yellow.

Fig 3: Electron microscopy characterization of Humanized Archaeoglobus *fulgidus* ferritin.
A) Sample micrograph of the HumAfFt data set. Scale bar: 100 nm.
B) Five representative 2D class averages obtained with RELION.
C) 3D reconstruction of HumAfFt obtained with RELION and visualized with UCSF Chimera (33). Map final resolution: 33.1 Å. Scale bars: 10 nm. Left: side view. Right: top view.
D) Archaeoglobus *fulgidus* ferritin crystal structure (from 16) filtered to 30 Å, shown for comparison. Scale bars: 10 nm. Left: side view. Right: top view.

Fig. 4: Humanized AfFt is internalized with higher efficiency than the original ferritin. Ferritins uptake in HeLa cells has been quantified by flow cytometry. Cells have been treated with 30µg/µl of AfFt-FITC, HumAfFt-FITC and transferrin-FITC (Tf). The percentage of cells internalizing the nanoparticles at the time indicated is shown. For each sample 30.000 events gated on live cells has been acquired.

Fig. 5: Ferritins internalization observed at the confocal microscope.

Cells were plated on 8-wells µ-slide (ibidi), induced with doxycycline to express TagRFP and then incubated with 30µg/µl of humanized AfFt-FITC or transferrin-FITC for 20h. After washing, cells were live-imaged at the confocal microscope. A) Confocal images of live HeLa TagRFP cells are

shown as single and merged channels and in the last column as overly with the phase contrast images. Scale bars: 40 μm. B) Images are a magnified view of the region highlighted by the white inset in panel A, merged channels and the overly with the phase contrast images are shown. Scale bars: 10 μm.

FIGURE 1

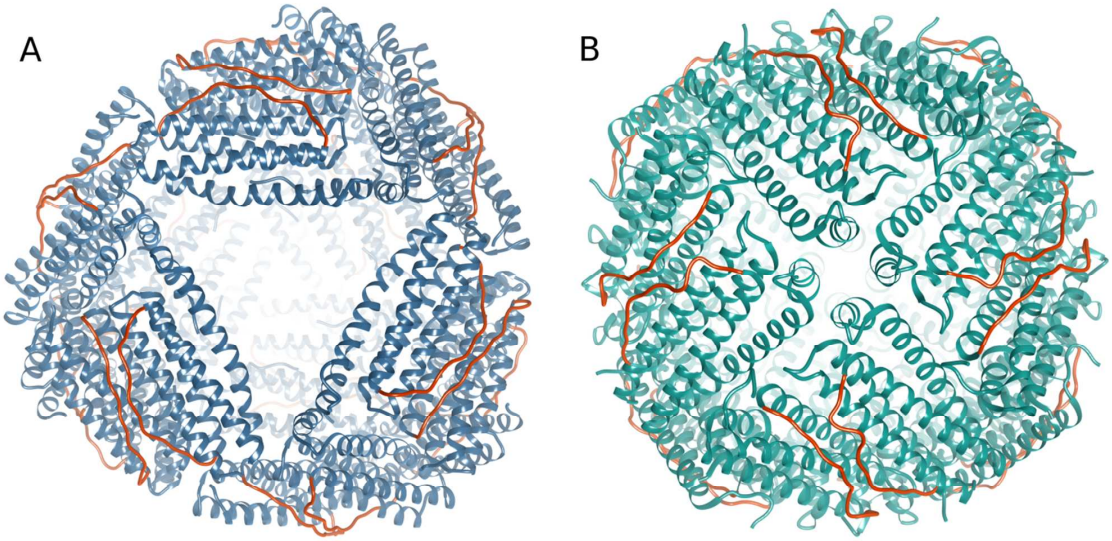

FIGURE 2

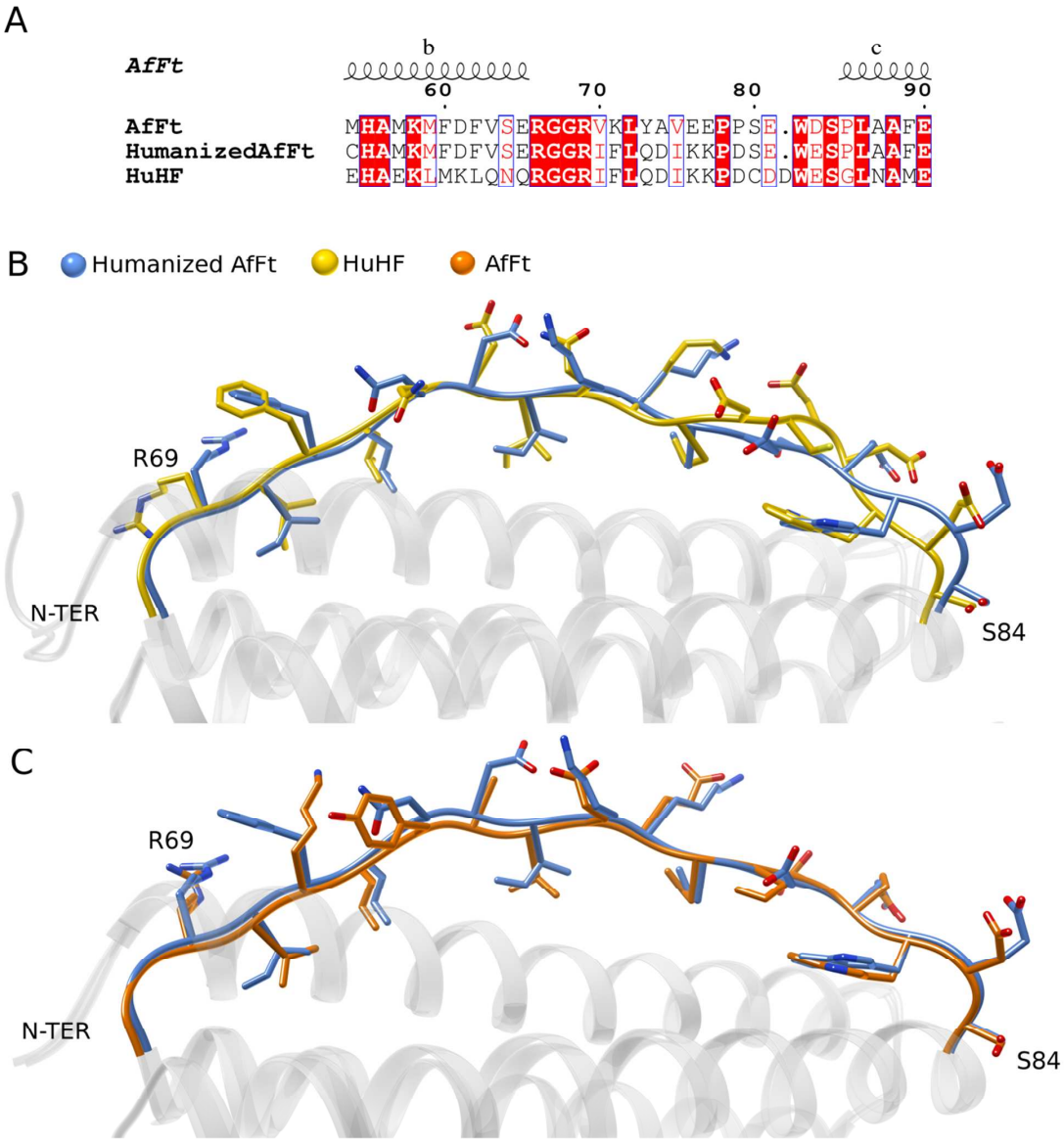
A
AfFt
b
c
60
70
80
90
AfFt
HumanizedAfFt
HuHF
B
Humanized AfFt
HuHF
AfFt
R69
N-TER
S84
C
R69
N-TER
S84

FIGURE 3

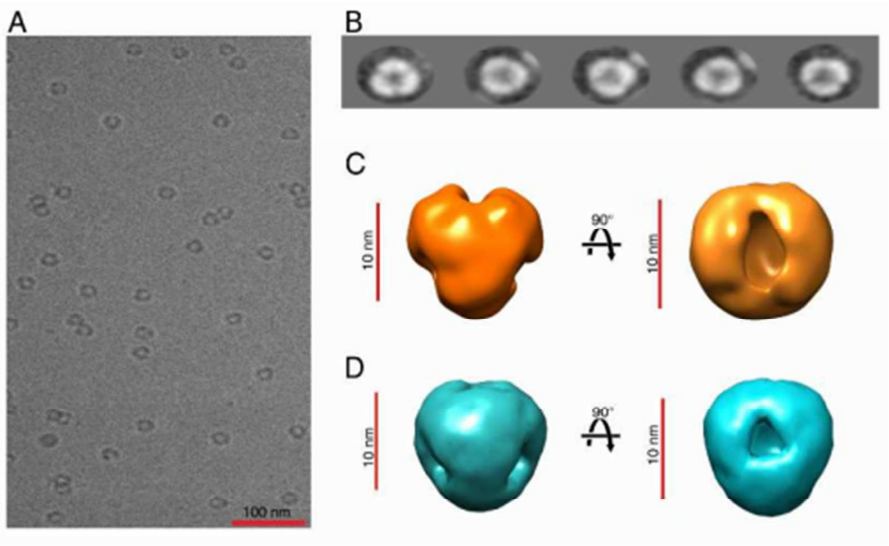

FIGURE 4

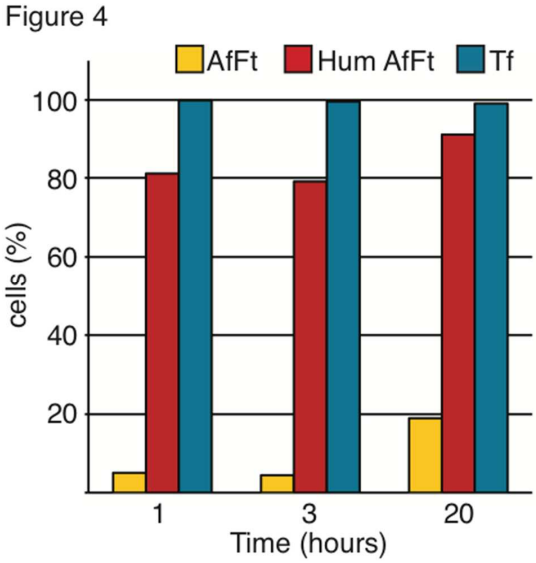

FIGURE 5

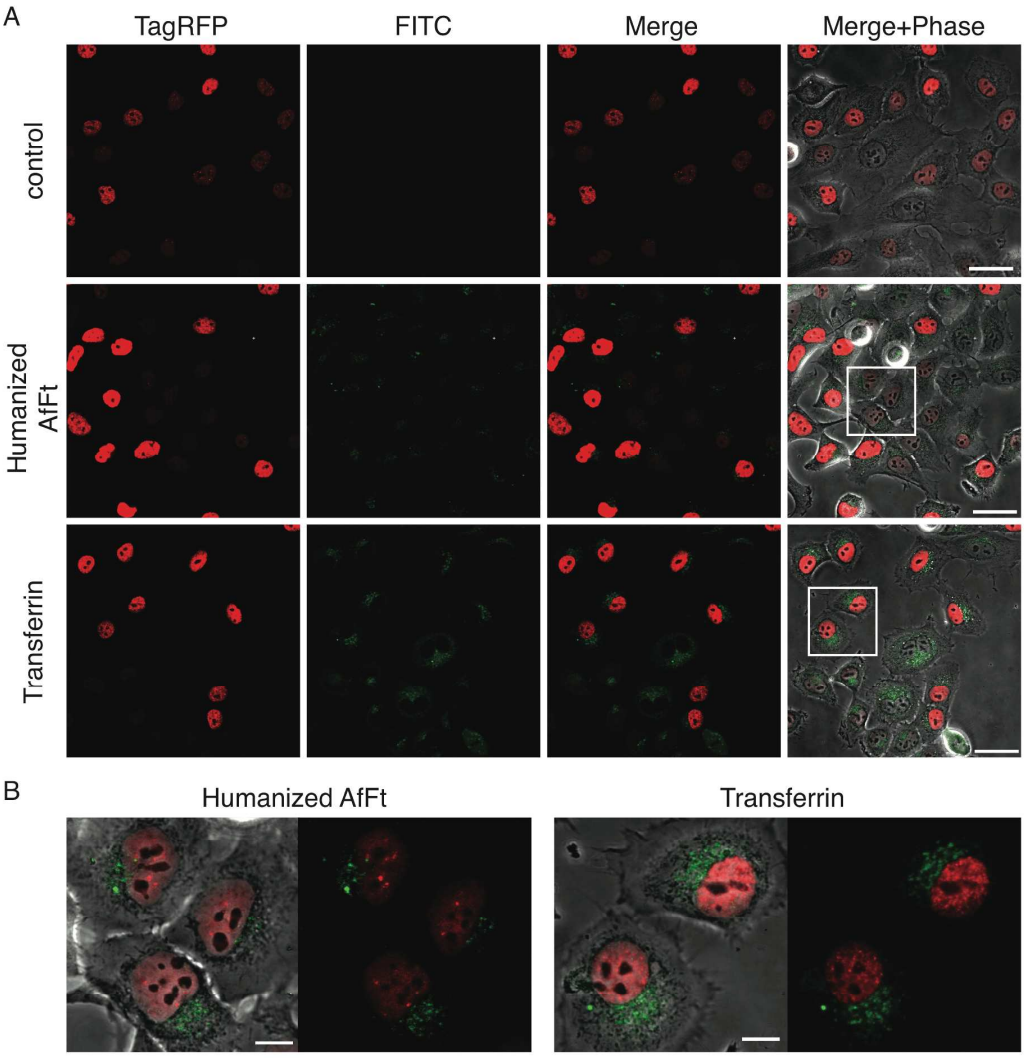
A
TagRFP
FITC
Merge
Merge+Phase
control
Humanized AfFt
Transferrin
B
Humanized AfFt
Transferrin

SUPPLEMENTARY INFORMATION.

Supplementary Materials

Humanized Archaeal ferritin as a tool for cell targeted delivery.

Valeria de Turris[a], Giovanna Peruzzi[a], Matilde Cardoso Trabuco[d], Alberto Boffi[a], Claudia Testi[a], Beatrice Vallone[c], Linda Celeste Montemiglio[b], Amédéede Georges[e], Lorenzo Calisti[b], Irene Benni[b], Alessandra Bonamore[b] and Paola Baiocco[a].

FigS1: Structure-based sequence alignment of AfFt, HumAfFt and HuHF.

Complete sequence alignment of AfFt, HumAfFt and HuHF. Elements of secondary structure for the AfFt are shown on the top. White characters in a red background indicate strict conservation while residues with poor conservation are drawn in black on a white background.

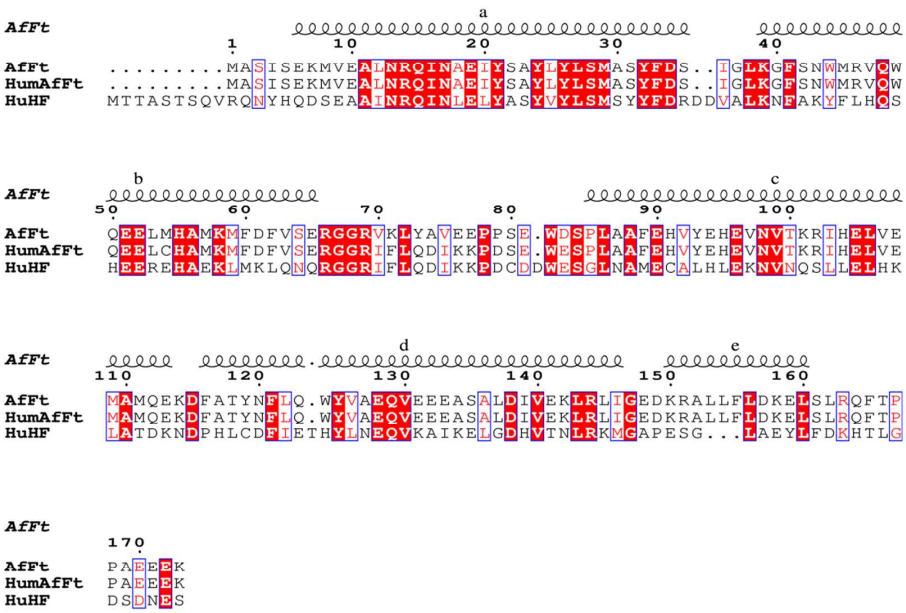

TABLE S1

Table S1: Data collection and refinement statistics[a]

[a]Numbers in parentheses refer to data in the highest resolution shell. R_{free} was computed omitting 5% of the reflections as a test set.

Data Collection	
Space Group	$C222_1$

Data Collection	
Space Group	$C222_1$
Cell Dimensions a, b, c (Å)	185.80 190.65 176.54
Resolution (Å)	48.86 - 2.94 (3.00 - 2.94)
R_{merge}	0.134 (0.751)
Unique Reflections	59926 (4378)
$I/\sigma I$	7.8 (1.8)
Completeness (%)	95.8 (95.6)
Redundancy	4.2 (4.3)
Refinement	
Resolution (Å)	49.69 - 2.94 (3.00 - 2.94)
No. reflections	56823 (346)
R_{factor} R_{free}	0.27 (0.61) 0.30 (0.59)
Ion (Mg^{2+})	2
water	13
R.m.s deviations	
Bond lengths (Å)	0,007
Bond angles (°)	0,99

FIGURE S2

Figure S2: Size exclusion chromatography profiles.

Chromatograms relative to the gel filtration profiles on Superdex 200 26/600 GL column of A) HumAfFt in 20 mM HEPES, pH 7.5, B) HumAfFt and C) AfFt in 20 mM HEPES, pH 7.5, 20 mM $MgCl_2$.

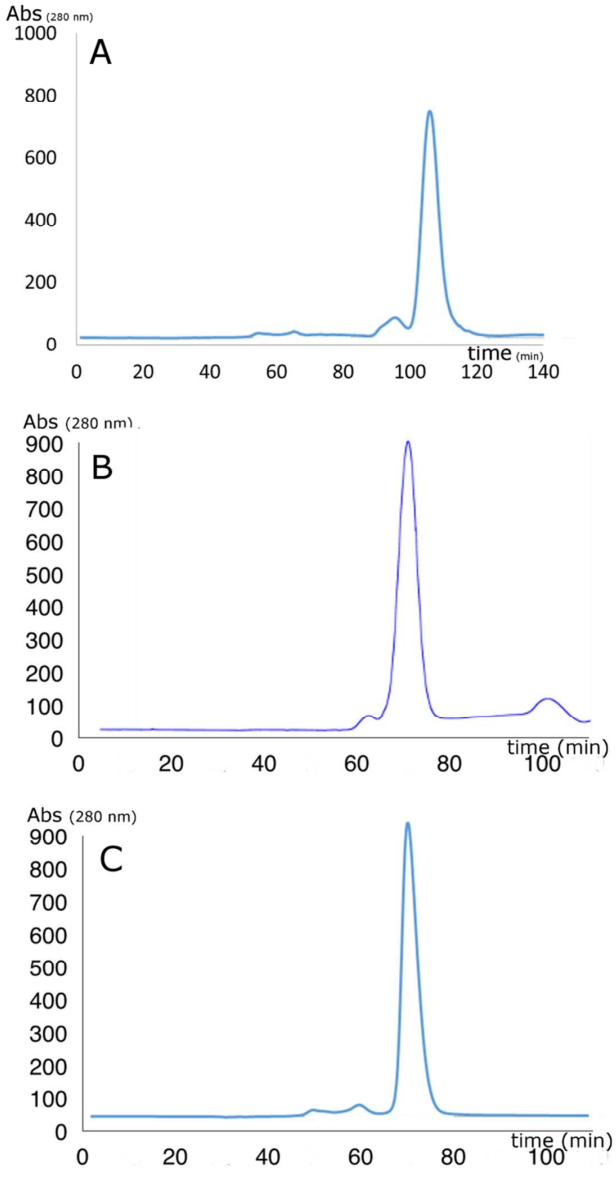

FIGURE S3

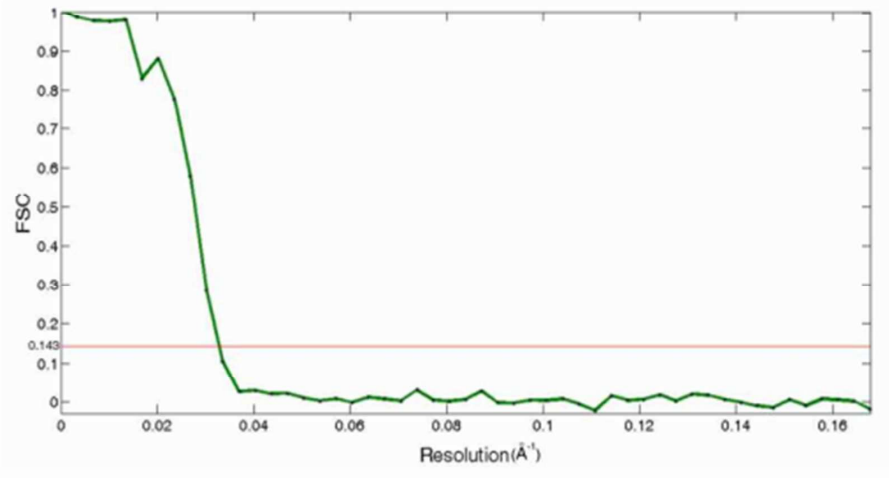

Supplementary Figure 3: Cryo-EM FSCs curve.

Gold standard Fourier Shell Correlation (FSC) curve of the HumAfFt three-dimensional reconstruction. Red line represents the resolution (equivalent to 33.1 Å) at which FSC=0.143.

FIGURE S4

FigureS4: **Ferritin internalization analysis by flow cytometry.**

Detailed FACS plot from the data presented in Fig.4. FACS analysis of HeLa cells show the increased uptake of HumAfFt compared to the original AfFt in the population at different time. Cells were treated and data were acquired as described in the Material and Methods section. As shown in the plots, the gate for the final detection was set in the control sample (CTRL) and the percentage of FITC positive cells for AfFt, HumAfFt and Transferrin (Tf) is indicated in each plot.

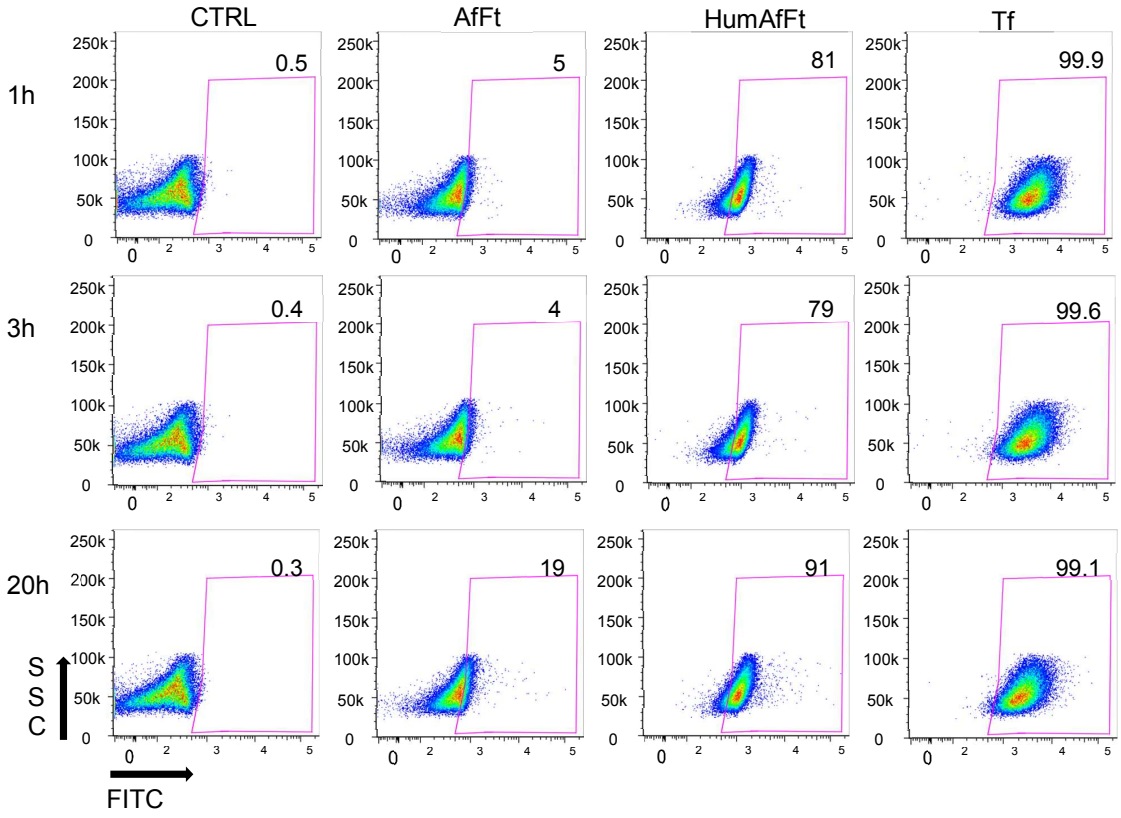

For each sample 30,000 events gated on live cells were acquired.

Author contribution:

All authors contributed extensively to the work presented in this paper. In detail, L.C. and I.B. expressed and purified the protein, A. Bonamore analysed the oligomerization state by GF chromatography, L.C.M., A.d.G. and C.T. performed and analysed EM experiments, M.T. performed crystallisation experiments and collected X Ray data, V.d.T. designed and performed internalization experiments on HeLa cells and confocal microscopy experiments, G.P. and V.d.T. performed and analysed FACS experiments, P.B. designed the chimeric protein and analysed X-Ray data, B.V. helped in critical revision of the manuscript and supervised EM experiments and A. Boffi supervised the project and prepared the manuscript. All authors discussed the results and commented the manuscript at all stages.